ELSEVIER

Earth and Planetary Science Letters 177 (2000) 131–140

EPSL

www.elsevier.com/locate/epsl

A dynamic origin for the global asymmetry of lunar mare basalts

Shijie Zhong [a,*], E.M. Parmentier [b], Maria T. Zuber [a]

[a] *Department of Earth, Atmospheric and Planetary Sciences, M.I.T., Cambridge, MA 02139, USA*
[b] *Department of Geological Sciences, Brown University, Providence, RI 02912, USA*

Received 5 October 1999; received in revised form 8 February 2000; accepted 9 February 2000

Abstract

We propose that the hemispheric asymmetry (Fig. 1) of mare basalts may be explained as a result of hydrodynamic instabilities associated with a layer of mixed ilmenite-rich cumulates (IC) and olivine–orthopyroxene (OPx) overlying a metallic core. This mixed layer (MIC) should form shortly after the solidification of the magma ocean (P.C. Hess and E.M. Parmentier, Earth Planet. Sci. Lett. 134 (1995) 501–514) because of gravitational differentiation of chemically dense IC material that is expected to form below the anorthositic crust in the final stages of magma ocean crystallization (A.E. Ringwood and S.E. Kesson, Proc. Lunar Planet. Sci. Conf. 7 (1976) 1697–1722). IC material is rich in heat producing elements, and thermal expansion due to radiogenic heating causes the MIC layer to become less dense than overlying mantle. The time required for the MIC layer to become thermally buoyant may explain a delay of mare volcanism until about 500 Ma after solidification of the magma ocean. Our analyses of the resulting Rayleigh–Taylor instability and numerical modeling of thermo-chemical convection show that the instabilities produce spherical harmonic degree 1 thermal and compositional structure if a lunar metallic core is sufficiently small, less than 250 km in radius.

Keywords: maria; volcanism; lunar interior; thermochemical properties; convection; differentiation

1. Introduction

The hemispheric asymmetry of mare basalts (Fig. 1; [1]) is fundamental to understanding the evolution of the Moon. The apparent correlation between mare and surface elevation had prompted the idea that mare basalt flooded topographically low areas. However, Clementine topographic data [4] indicate that while mare basalts clearly fill low areas, large areas of low elevation do not contain mare basalt. The nearside–farside crustal thickness asymmetry has been considered responsible for the center of figure-center of mass offset of the Moon. The crustal asymmetry approximately coincides, but only approximately, with the hemispheric asymmetry of mare basalts. This has led to the suggestion that endogenic processes that produce the crustal thickness asymmetry might also subsequently control the mare distribution [5]. A previous study [6] suggested that the crustal asymmetry may be related to the formation of a

* Corresponding author. Tel.: +1-617-253-3748; Fax: +1-617-258-9697; E-mail: szhong@rayleigh.mit.edu

0012-821X/00/$ – see front matter
PII: S0012-821X(00)00041-8

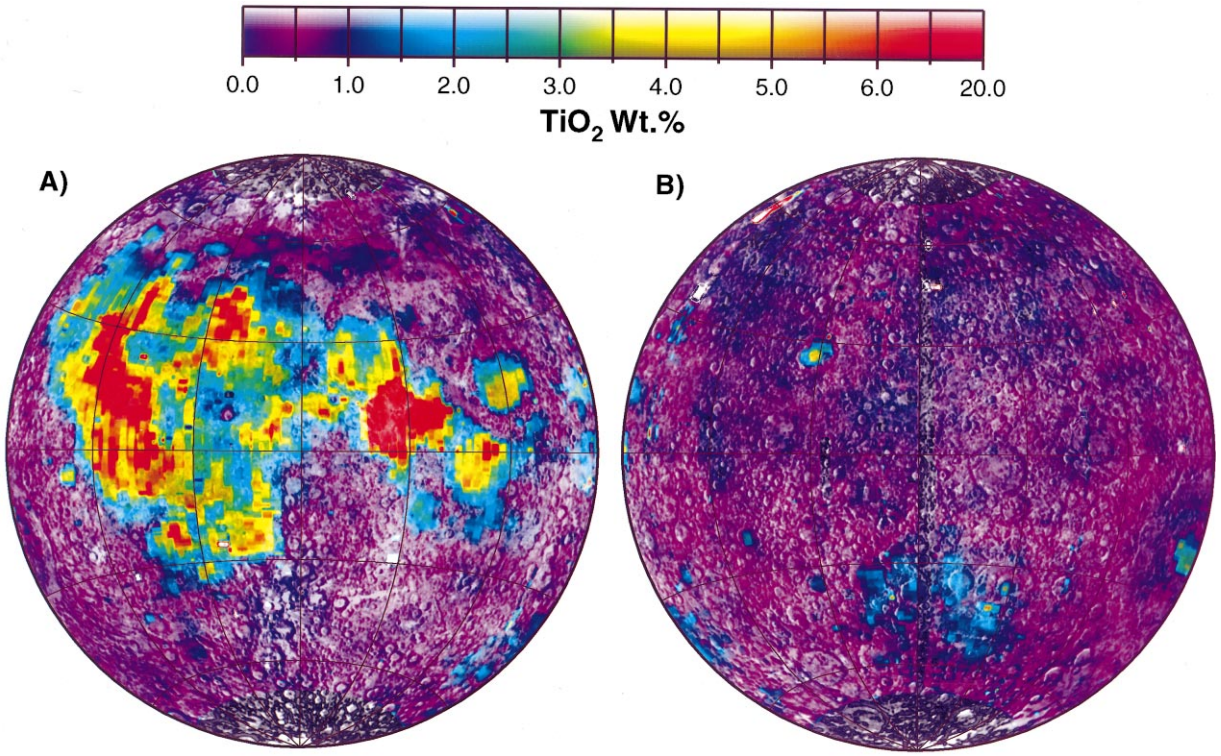

Fig. 1. The surface distribution of TiO_2 on the (A) nearside and (B) farside of the Moon [1]. High concentration of TiO_2 is indicative of mare basalts.

metallic core at the very early stage of lunar evolution. However, this study did not address the timing and distinct geochemical signatures of mare basalts. On the other hand, a particularly simple explanation of the crustal thickness asymmetry is that it may be a consequence of the redistribution of crustal material excavated from the SP-Aitken basin [4] and therefore unrelated to the endogenic processes that created the mare basalts.

Rare earth element (REE) distributions in the mare basalts are complementary to those in anorthositic crust [7]. This has generally been interpreted as showing that mare basalts were derived by remelting materials that crystallized contemporaneously with the anorthositic crust [7], presumably near its base at depths shallower than 100 km. The anorthositic crust is thought to have formed by fractional crystallization of a magma ocean [7]. Ilmenite-rich pyroxene cumulates (IC) with a greater density than underlying olivine–orthopyroxene (OPx) mantle are expected to have crystallized from residual liquid beneath the anorthositic crust after about 90% of magma ocean has solidified [2,8]. This IC material should contain a high concentration of incompatible elements including heat producing U and Th as well as REE with distributions complementary to the anorthositic crust [7]. But mare basalts are thought to originate from source regions at depths greater than 400–600 km [9] so that at least some differentiation of late-stage magma ocean cumulates to the deeper interior is required.

Previous studies [2,3,10,11] have suggested that solid state creep flow would allow dense IC materials to sink into the deep interior. However, this differentiation is likely to be complex. Solid IC crystallizing from the residual magma ocean liquid will settle through the underlying OPx mantle at a rate determined by its creep viscosity and by the size of the dense diapirs or plumes. Small, slowly settling dense bodies forming from a thin IC layer will create a mixed layer that itself be-

comes unstable at larger scales allowing differentiation to proceed more rapidly [2,12]. If the Moon was formed by the accretion of cold planetesimals, an initially cold, high viscosity deep interior might inhibit the sinking of the dense mixed layer. However, if the Moon formed by an early giant impact with the Earth [13], it is expected to be initially hot throughout. Even if the viscosity of the deep mantle is relatively low, a reduced creep rate due to cooling could strand a significant fraction of the IC material near the base of the anorthositic crust, thus creating the KREEP layer thought to be present in the Moon. But it is reasonable to suppose [2,12] that some fraction of the IC material differentiated into the deep interior as required to generate Ti-rich mare basalts by deep melting. Finally, the concentration of incompatible heat producing elements in the IC will be determined by the amount of intragranular liquid retained in the cumulate and will increase with the degree of fractionation of the residual liquid [12].

After its gravitational differentiation, this mixed material will very likely form a layer of mixed IC and OPx (MIC) overlying a metallic core. The evolution of this MIC layer may hold the key to understanding the genesis of mare basalts. The layer is initially stable, because MIC materials are chemically denser than the overlying olivine–pyroxene mantle. However, the MIC layer, as it heats up due to its relatively high content of U and Th, will become unstable when thermal expansion offsets its negative compositional buoyancy. Buoyant MIC materials will ascend and undergo decompression melting, potentially giving rise to mare basalt volcanism that originates from deep melting. Our objective is to examine the conditions for instability and the resulting wavelengths at which it would occur.

2. Model description

Because of the complexity of the differentiation, we examine a range of models with three adjustable parameters. We will identify the regions of this parameter space in which a hydrodynamic instability produces hemispheric asymmetric (i.e. degree 1) structure and the time that it would take for this to occur. The first parameter is the rate of heat production H_{IC}. We consider IC cumulates

Table 1
Model parameters

Radii of the Moon R_o	1.74×10^6 m
Density of peridotitic mantle ρ_M	3400 kg m^{-3}
Density of ilmenite cumulate ρ_{IC}	3700 kg m^{-3}
Heat production rate for bulk Moon	$H_B(t)$[a]
Concentration of uranium	25.7 PPB
Thermal expansivity for	
solids	3×10^{-5} K^{-1}
liquids	1×10^{-4} K^{-1}
Thermal diffusivity	10^{-6} m^2 s^{-1}
Thermal conductivity	4.0 W K^{-1} m^{-1}
Surface gravitational acceleration	1.63 m s^{-2}
Adiabatic temperature gradient	0.03 K MPa^{-1}
Melting temperature gradient	0.1 K MPa^{-1}
Rheology[b]	
$\eta=\eta_0\exp[E+PV/RT]$	
Activation energy E	1.5×10^5 J mol^{-1}
Activation volume V	6×10^{-6} m^3 mol^{-1}
Reference viscosity η_0	10^{19} Pa s

[a] $H_B(t)$ is the bulk mantle heat production rate and is determined with Th/U = 4 and K/U = 2000, and appropriate decay times and concentration for each radioactive element [15].

[b] The rheology for silicate rocks is predominantly temperature-dependent [16]. The activation energy used in this study is about half of that measured for dry olivine, but the reduced value may be consistent with that inferred from flexural rigidity near seamounts and oceanic islands [17].

that represent 5% of the volume of the Moon, probably a reasonable upper bound if the Moon was initially fully molten [2,7]. Heat producing elements, predominantly U and Th, are highly incompatible and become concentrated in the residual liquid of the magma ocean. The amount of these elements incorporated into the IC must depend on the amount of trapped intragranular liquid in the cumulates [12]. Given the variable and uncertain amount of incompatible elements in the IC, we examine rates of heat production H_{IC} in the range of 10–20 times that of the bulk Moon H_B (see Table 1), the larger value corresponding to all of the heat production in the Moon concentrated in the last 5% residual liquid. Since the Moon is depleted in K, H_B is assumed to be the same as that which would be generated by U and Th in the Earth's mantle (Table 1), as seems reasonable for a giant impact origin. A smaller value of H_{IC} is certainly conceivable but probably would not allow mare volcanism to occur early enough in the evolution of the Moon.

The second parameter is the concentration c of IC cumulates in the MIC. A value $c = 0.2$ is suggested by a simple analysis of differentiation [12]. The rate of heat production in the MIC is cH_{IC}. The compositional density difference between IC and OPx mantle $\Delta\rho_{IC}$ is about 8.8% [2] and that for the MIC material is reduced by a factor of c. The value of ρ_{IC} which we have used (Table 1) is based on estimates that the ilmenite/pyroxene ratio in the IC is about 1/3 [2,7]. More ilmenite-rich compositions would result in an even higher density. We also introduce a parameter f that represents the fraction of IC cumulates that are differentiated into deeper interior, the fraction $(1-f)$ forming a KREEP layer that remains near the base of the crust. The ratio of the volume of the mixed layer to the volume of IC is thus f/c. This ratio determines the radius of the mixed layer $R_{MIC} = (0.05R_o^3 f/c + R_i^3)$, where R_i and R_o are the radii of the metallic core and the Moon, respectively. With $f = 0.5$ and $c = 0.2$, the radius of the mixed layer would be about half of the radius of the Moon if no metallic core or one with a negligible volume was present.

We will use two different techniques to examine the conditions for instability and the resulting wavelengths: a Rayleigh–Taylor (R–T) instability analysis and finite element modelling of thermo-chemical convection. With the R–T instability analysis, we will determine the wavelengths at which the mixed layer goes unstable. For this purpose, we assume that the MIC layer is already unstable with a density that is smaller than the overlying mantle, and then we calculate growth rates for different wavelengths or spherical harmonics. The growth rates of small amplitude perturbations are determined with an analytical approach that was originally developed for studying stress relaxation associated with impact basins [14]. Like previous R–T instability analyses [15], thermal effects are excluded and the displacement at density interfaces is assumed to be small which enables us to linearize the boundary condition. While previous analyses are often done for isoviscous flow in a Cartesian geometry [15], our R–T instability analysis works for both isoviscous and layered viscosity structure for a spherical geometry.

To understand the relative roles of thermal and chemical buoyancy, we will use finite element models of thermo-chemical convection in a spherically axisymmetric geometry [16]. Our thermo-chemical convection models are based on the following assumptions:

1. The models treat two initially compositionally distinct layers: a layer of OPx mantle and an underlying MIC layer. The crust and the KREEP layer are not explicitly included, because the viscosity is relatively large due to the low temperature at these shallow depths. However, the thermal blanketing effect of the KREEP layer is considered.
2. Heat production rates are cH_{IC}, 0 and H_{IC} for the mixed layer, the mantle and KREEP layer, respectively. Various model parameters are presented in Table 1.
3. The initial temperature profile follows an adiabat with a potential temperature equal to the solidus temperature at the crust–mantle boundary (Table 1). For boundary conditions, the surface is free-slip and isothermal; the core–mantle boundary is free-slip and thermally insulating. A free-slip condition at the core–man-

tle boundary assumes that the metallic core is liquid. As the MIC layer heats up, we neglect heating of the core.

4. Temperatures in our models may become high enough to cause partial melting. IC inclusions will melt at a ~100 K lower temperature than the host, generating melts that are denser than the host [17]. If no reaction occurred between IC and host, the volume increase of the melted IC would result in a reduced bulk density of MIC. However, reactions between the IC melt and host that occur by infiltration or diffusion will increase the Fe and Ti content of minerals in the host [3], thus increasing its density and largely offsetting the loss of dense mineral phases in the IC. The small density decrease that may occur is difficult to calculate based on available mineral physics data. Here, we make the simple assumption that IC melts are consumed by reaction with the host with no overall change in the density contrast between the MIC materials and the mantle. If temperatures exceed the host solidus, volume expansion due to melting will reduce the overall density by an amount that depends on the degree of melting. We represent this as an increased effective thermal expansion coefficient of 10^{-4} K^{-1}, corresponding to a 5% volume increase distributed linearly over the 500 K interval between the peridotite solidus and liquidus.

3. Results

In this section, we will first demonstrate the conditions under which degree 1 structure may develop by using a R–T instability analysis. We will then present finite element thermo-chemical convection models to show how radioactive heating within the MIC layer can lead to the instabilities that produce degree 1 distribution in both thermal and compositional structures.

3.1. Degree 1 instability from a R–T instability analysis

For a two layer system in a Cartesian geometry in which the top layer has a greater density, instabilities will occur at a wavelength that depends on the layer thickness [15]. In a spherical geometry, we will demonstrate that the preferred wavelengths for instabilities depend on not only the layer thickness but also the inner radius R_i of

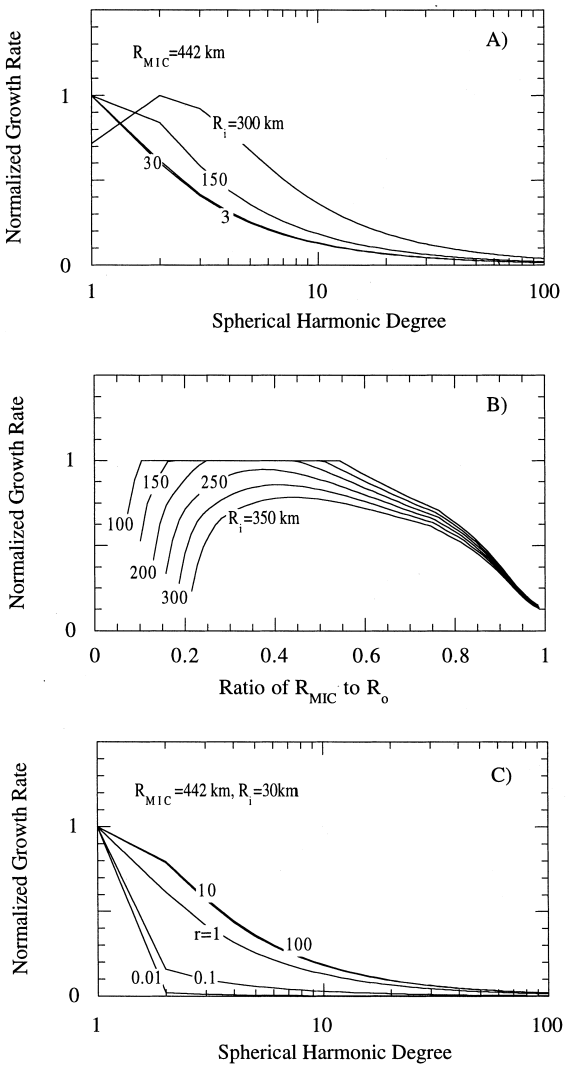

Fig. 2. (A) Dependence of normalized growth rate on harmonic degrees for models with a different inner radius R_i. (B) Dependence of normalized growth rate at degree 1 on R_i and the radius of mantle–MIC boundary R_{MIC}. (C) Dependence of normalized growth rate on harmonic degrees for models with a different ratio of mantle viscosity to MIC viscosity, r.

the bottom layer (i.e. MIC layer) [18–20]. For a given viscosity structure, density difference across the boundary between MIC and mantle, R_i and R_{MIC}, a growth rate for instabilities, can be calculated for each wavelength or spherical harmonic with an analytic approach that is developed in [14]. The dominant wavelength will be the one with the fastest growth rate.

Our analyses have shown that the dominant wavelengths depend on R_i, R_{MIC} and the viscosity structures of the mantle and MIC layer. When $R_i = 300$ km, $R_{MIC} = 444$ km and the MIC layer and the mantle have the same viscosity, the fastest growth rate occurs at degree 2 (Fig. 2A). However, as R_i is reduced with other parameters fixed, degree 1 becomes the fastest growing mode (Fig. 2A). If R_i is fixed at 300 km, degree 1 cannot be the fastest mode no matter how thick the MIC layer is (Fig. 2B). This is because as the layer thickness or R_{MIC} increases, the longest wavelength will be limited by the resisting stress on the surface boundary at R_0. Our analysis shows that for isoviscous mantle and MIC layer, the fastest growth rate occurs at degree 1 for a range of MIC layer thicknesses (Fig. 2B) but only for a sufficiently small metallic core ($R_i < 250$ km). If the MIC layer is less viscous than the overlying mantle, the growth rate for $l = 1$ mode remains the fastest over a large parameter space. However, the difference in growth rate between the $l = 1$ mode and modes at higher l is reduced (Fig. 2C). A MIC layer more viscous than the overlying mantle enhances the $l = 1$ mode (Fig. 2C).

3.2. Generation of degree 1 structure from thermo-chemical convection

We now demonstrate how the MIC layer becomes unstable due to radioactive heating and how the instabilities may lead to degree 1 distribution in both thermal and compositional structures. The minimum thermal buoyancy and time scale for the instability to occur can be simply estimated. For a mixed layer with IC concentration c, the relative density difference between MIC materials and the mantle is $c\Delta\rho_{IC}$, and the temperature difference for the MIC layer to offset its compositional buoyancy is $c\Delta\rho_{IC}/\alpha$, where α is the thermal expansivity. For the heat production rate H_B (Table 1), the temperature increase is about 0.5 K Ma^{-1}. With the heat production rate cH_{IC}, the time needed for the MIC layer to reach neutral buoyancy is independent of c. For $\Delta\rho_{IC} = 8.8\%$, $H_{IC} = 20H_B$ and $\alpha = 3\times10^{-5}$ K^{-1}, neutral buoyancy is attained after 293 Ma and, for $c = 0.2$, with a minimum temperature increase of 587 K. Thermal diffusion will act to damp instability so that additional thermal buoyancy, depending on the mantle viscosity, is needed before the MIC layer becomes unstable.

Our thermo-chemical convection models use a field method for advecting the composition [16]. In order to achieve accurate solutions for the field method, a high resolution is necessary [21]. We use 120 and 180 elements in the radial and azimuthal directions, respectively, with finer grids within the MIC layer and in the mantle near the compositional boundary. Our numerical tests show

Table 2
Onset time and temperature and dominant structure

H_{IC}/H_B	c	Onset time (Ma)	Onset temperature (°C)	Structure l
20	0.1	438 (294)[a]	1643 (1529)	1
	0.2	348 (274)	1911 (1777)	1
	0.3	270 (221)	2040 (1904)	1
10	0.1	651 (695)	1515 (1530)	2
	0.2	629 (638)	1798 (1802)	2
	0.3	562 (497)	2010 (1937)	1

[a]The numbers in parentheses are the time and temperature for the MIC layer to reach a neutral buoyancy with respect to the overlying mantle in the model.

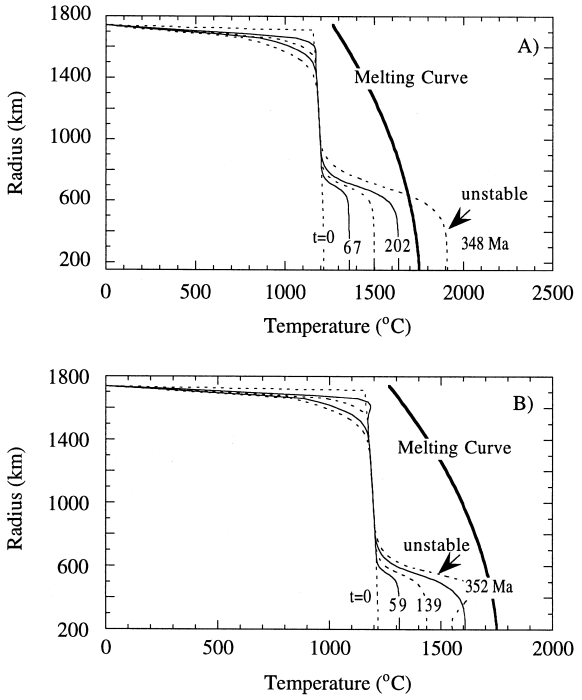

Fig. 3. Dependence of azimuthally average temperature on radius at different times for (A) model 1 with constant viscosity and (B) model 2 with temperature-dependent viscosity. The melting curve shows temperatures appropriate for the generation of lunar volcanic glasses. IC inclusions would initially melt at temperatures that could be several hundred degrees lower.

that this resolution is sufficient and that our results are robust, particularly for the relatively short integration time (i.e. half overturn time) that we are interested. We have considered models with both constant viscosity and temperature-dependent viscosity.

Our first example considers a constant 5×10^{20} Pa s viscosity; $c=0.2$; $H_{IC}=20H_B$; $R_i=150$ km; and $R_{MIC}=690$ km (i.e. $f=25\%$). As the MIC layer heats up, a conductive thermal boundary layer forms near the MIC–mantle boundary, but no thermal convection occurs (Figs. 3A and 4A). After 270 Ma, the temperature in the bottom part of the MIC layer exceeds the melting temperature. At 274 Ma, the MIC layer becomes neutrally buoyant (Table 2), but the layer remains stable. At 348 Ma, with continued heating and thermal expansion, the MIC layer becomes unstable (Fig.

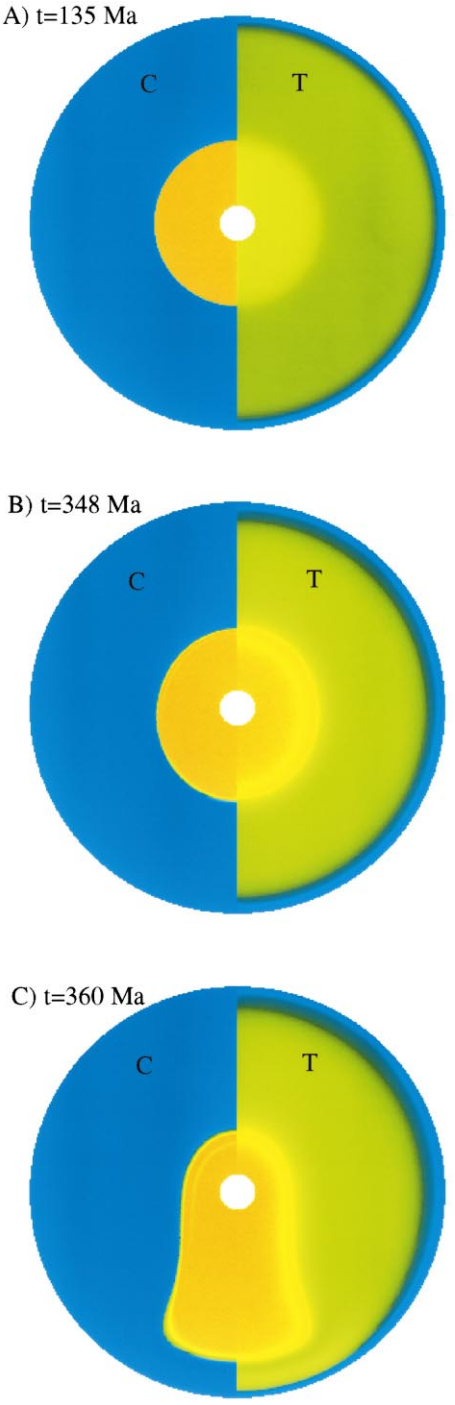

Fig. 4. Temperature (T and the left panel) and compositional (C and the right panel) fields at different times for (A, B, C) model 1 with constant viscosity.

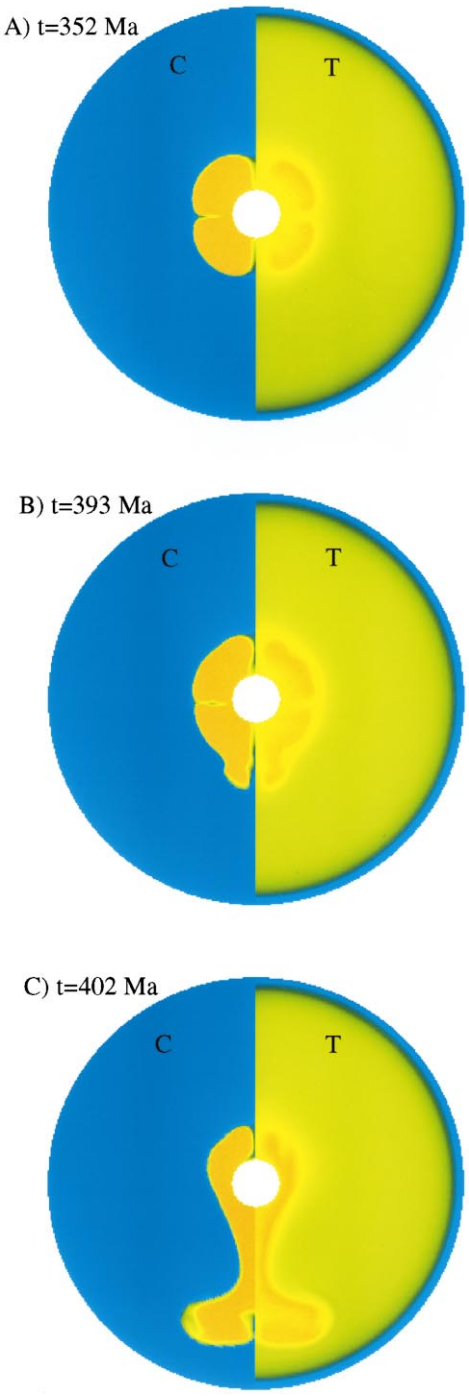

Fig. 5. Temperature (T and the left panel) and compositional (C and the right panel) fields at different times for (A, B, C) model 2 with a temperature-dependent viscosity.

3A). As the instability grows, the MIC moves to one hemisphere, forming $l=1$ thermal and compositional structure (Fig. 4B,C). As in the simpler R–T stability analysis (Fig. 2B), the numerical models show that the dominant wavelength critically depends on R_i and R_{MIC}. For example, for $R_i = 300$ km, only degree 2 and 3 structures can be generated.

We have explored the sensitivity of the onset time and temperature (i.e. the maximum temperature when MIC layer becomes unstable) and the dominant structure to c and H_{IC} for models with the same R_i and R_{MIC} as those in the first model. For a given H_{IC}, onset temperature increases with c, but onset time decreases with c (Table 2). A larger c corresponds to larger compositional buoyancy which results in a larger onset temperature. The decreasing onset time with increased c is primarily caused by the increased expansion coefficient after the MIC temperature exceeds the melting temperature (Table 2). Smaller H_{IC} (e.g. $H_{IC} = 10H_B$) results in a longer onset time because the MIC layer with smaller H_{IC} heats up more slowly. The onset temperature is smaller for smaller H_{IC}, particularly for $c = 0.1$ and 0.2 (Table 2). A smaller H_{IC} takes longer to create a given temperature difference between the MIC layer and mantle, giving more time to create a thicker diffusive thermal boundary layer. Therefore, it requires less thermal buoyancy to destabilize the MIC layer for smaller H_{IC}. We also found that while the dominant structure is always degree 1 for $H_{IC} = 20H_B$, degree 2 occurs only for $c = 0.1$ and 0.2 and $H_{IC} = 10H_B$ (Table 2). For $c = 0.1$ and 0.2 and $H_{IC} = 10H_B$, the onset times and temperatures are smaller than those for reaching neutral buoyancy (Table 2), suggesting that the instabilities are mainly caused by the thermal boundary layer rather than the MIC buoyancy. We have also considered models with a higher 5×10^{21} Pa s mantle viscosity. The higher mantle viscosity increases both onset time and temperature, as expected. Although the thermal boundary layer is thicker, the dominant structure of instabilities remains the same as that from calculations with smaller viscosity.

Our second model with temperature-dependent viscosity shows that degree 1 instability can occur

at subsolidus temperature. In this case, $c = 0.15$; $H_{IC} = 20H_B$; $R_i = 200$ km; and $R_{MIC} = 560$ km ($f = 10\%$). The viscosity at the melting temperature at core–mantle boundary pressure is 10^{19} Pa s, and the activation energy is 150 kJ mol^{-1} (Table 1). As the temperature increases, the mantle and MIC viscosities decrease. At 352 Ma, thermal convection develops within the MIC layer (Fig. 5A). However, during this period, the MIC layer is stable with respect to the overlying mantle (Fig. 5A). After 390 Ma, the entire MIC layer becomes buoyant and moves towards one hemisphere while thermal convection is still occurring within the MIC layer. This subsequently results in a predominantly degree 1 structure (Fig. 5B,C), but with smaller-scale features inherited from the thermal convection. In this model, the temperature within the MIC layer is below the melting temperature when the degree 1 instability occurs (Fig. 3B). However, as the MIC material rises, decompression melting would occur.

4. Discussion

As discussed earlier, the lunar crustal thickness asymmetry may result from redistribution of crustal material excavated from the SP-Aitken impact basin. However, it might be argued that the degree 1 instability from our models may produce a similar crustal thickness variation depending on the thermal and mechanical structure of the crust when the instability occurs. Creep flow in the lower crust may occur at a much lower temperature than it does in the mantle [22], and if the lower crust can flow when instability occurs, the degree 1 mantle flow may lead to crustal thinning in the hemisphere with upwelling and crustal thickening in the other hemisphere. Although the thick lunar crust ($\sim$55 km) would favor flow in the lower crust, studies of elastic lithosphere thickness near lunar basins filled with mare basalt suggest an elastic layer at least 50 km at the time that mare basalts were emplaced [23]. Crustal flow could be important only if the elastic lithosphere was thinner than these earlier estimates indicate.

We have demonstrated that hydrodynamic instabilities of a mixed layer of IC and OPx above a metallic core may generate the hemispherical asymmetry in thermal and compositional structures that may explain the temporal and spatial distributions of mare basalts. The key parameters include the radii of metallic core R_i and mantle–MIC boundary R_{MIC}. Moment of inertia from Lunar Prospector constrains R_i to fall between 220 km and 450 km [24]. However, a smaller R_i is also allowed by the moment of inertia [2]. The historical record of lunar laser ranging data indicates a maximum core radius in the range of 220–350 km [25], with most recent results yielding a one-sigma upper limit of 352 and 374 km for Fe and FeS core compositions, respectively [26]. Recent analysis of magnetometer data from Lunar Prospector strongly excludes core radii greater than 450 km with cores smaller than 300 km less strongly excluded [27]. When all uncertainties are considered, laser ranging and induced magnetic moment observations imply only an upper bound on core radius (352–425 km) [28]. R_{MIC} depends on how the IC differentiates. However, the range of R_i and R_{MIC} over which degree 1 can be generated (Fig. 2B) is large enough to satisfy the observational constraints and a variety of differentiation models.

Acknowledgements

Thanks to L. Kellogg for allowing the use of the finite element code SCAM. This research is supported by NASA Grants NAG5-3659 and NAGW-5021.*[RV]*

References

[1] P.G. Lucey, D.T. Blewett, B.R. Hawke, Mapping the FeO and TiO_2 content of the lunar surface with multispectral imagery, J. Geophys. Res. 103 (1998) 3679–3699.
[2] P.C. Hess, E.M. Parmentier, A model of the thermal and chemical evolution of the Moon's interior: Implications for the onset of mare volcanism, Earth Planet. Sci. Lett. 134 (1995) 501–514.
[3] A.E. Ringwood, S.E. Kesson, A dynamic model for mare basalt petrogenesis, Proc. Lunar Planet. Sci. Conf. 7 (1976) 1697–1722.
[4] M.T. Zuber, D.E. Smith, F.G. Lemoine, G.A. Neumann,

The shape and internal structure of the Moon from the Clementine mission, Science 266 (1994) 1839–1843.
[5] J.T. Wasson, P.H. Warren, Contribution of the mantle to the lunar asymmetry, Icarus 44 (1980) 752–771.
[6] D.J. Stevenson, Lunar asymmetry and palaeomagnetism, Nature 287 (1980) 520–521.
[7] R.S. Taylor, Planetary Science: A Lunar Perspective, Lunar Planet. Inst., Houston, TX, 1982, 481 pp.
[8] G.A. Snyder, L.A. Taylor, C.R. Neal, A chemical-model for generating the sources of mare basalts-combined equilibrium and fractional crystallization of the lunar magmasphere, Geochim. Cosmochim. Acta 56 (1992) 3809–3823.
[9] J.W. Delano, Pristine lunar glasses-criteria, data, and implications, J. Geophys. Res. 91 (1986) 201–213.
[10] F.J. Spera, Lunar magma transport phenomena, Geochim. Cosmochim. Acta 56 (1992) 2253–2266.
[11] F. Herbert, Time-dependent lunar density models, Proc. Lunar Planet. Sci. Conf. 11 (1980) 2015–2030.
[12] E.M. Parmentier, P.C. Hess, On the chemical differentiation and subsequent evolution of the Moon, Lunar Planet. Sci. Conf. 30 (1999) 1289–1290.
[13] A.G.W. Cameron, The origin of the moon and the single impact hypothesis, Icarus 126 (1997) 126–137.
[14] S. Zhong, M.T. Zuber, Long-wavelength topographic relaxation for self-gravitating planets and implications for the time-dependent compensation of surface topography, J. Geophys. Res. 105 (2000) 4153–4164.
[15] H. Ramberg, Deformation of the Earth's Crust in Theory, Experiments and Geological Application, 2nd edn., Academic Press, San Diego, CA, 1981, 452 pp.
[16] L. Kellogg, S.D. King, Effect of mantle plumes on the growth of d by reaction between the core and mantle, Geophys. Res. Lett. 20 (1993) 379–382.
[17 J.W. Delano, Buoyancy-driven melt segregation in the earths moon. 1. numerical results, Proc. Lunar Planet. Sci. Conf. 20 (1990) 3–12.
[18] D.L. Turcotte and G. Schubert, Geodynamics, John Wiley, New York, 1982.
[19] S. Karato, P. Wu, Rheology of the upper mantle: A synthesis, Science 260 (1993) 771–778.
[20] A.B. Watts, S. Zhong, Observations of flexure and the viscoelastic properties of the lithosphere, EOS Trans. Am. Geophys. Un. 79 (Suppl.) (1998) 911.
[21] P.E. van Keken, S.D. King, H. Schmeling, U.R. Christensen, D. Neumeister, M.-P. Doin, A comparison of methods for the modeling of thermochemical convection, J. Geophys. Res. 102 (1997) 22477–22495.
[22] N.L. Carter, M.C. Tsenn, Flow properties of continental lithosphere, Tectonophysics 136 (1987) 27–63.
[23] S.C. Solomon, J.W. Head, Lunar mascon basins: lava filling, tectonics, and evolution of the lithosphere, Rev. Geophys. Space Phys. 18 (1980) 107–141.
[24] A.S. Konopliv, A.B. Binder, L.L. Hood, A.B. Kucinskas, W.L. Sjogren, J.G. Williams, Improved gravity field of the Moon from Lunar Prospector, Science 281 (1998) 1476–1480.
[25] J.O. Dickey et al., Lunar laser ranging: A continuing legacy of the Apollo program, Science 265 (1994) 482–490.
[26] J.G. Williams, D.H. Boggs, J.T. Ratcliff and J.O. Dickey, The Moon's molten core and tidal Q, Lunar Planet. Sci. Conf. XXX, Lunar and Planet. Inst., Houston, TX, 1999.
[27] L.L. Hood, R.P. Lin, D.L. Mitchell, M.H. Acuna and A.B. Binder, Initial measurements of the lunar induced magnetic moment in the geomagnetic tail using Lunar Prospector data, Lunar Planet. Sci. Conf. XXX, Lunar and Planet. Inst., Houston, TX, 1999.
[28] L.L. Hood and M.T. Zuber, Recent refinements in geophysical constraints on lunar origin and evolution, Submitted to Origin of Earth and Moon, Univ. of Ariz. Press, Tucson, AZ, 1999.